BIOCHEMISTRY
including biophysical chemistry & molecular biology
Article

Biochemistry **2010,** *49,* 6945–6952 6945
DOI: 10.1021/bi100892w

The Three-His Triad in Dke1: Comparisons to the Classical Facial Triad†

Adrienne R. Diebold,‖ Michael L. Neidig,‖ Graham R. Moran,‡ Grit D. Straganz,*,§ and Edward I. Solomon*,‖

‡*Department of Chemistry and Biochemistry, University of Wisconsin, Milwaukee, Wisconsin 53211,* §*Institute for Biotechnology and Biochemical Engineering, Graz University of Technology, Petersgasse 12, A-8010 Graz, Austria, and* ‖*Department of Chemistry, Stanford University, Stanford, California 94305*

Received June 2, 2010; Revised Manuscript Received July 13, 2010

ABSTRACT: The oxygen activating mononuclear non-heme ferrous enzymes catalyze a diverse range of chemistry yet typically maintain a common structural motif: two histidines and a carboxylate coordinating the iron center in a facial triad. A new Fe^{II} coordinating triad has been observed in two enzymes, diketone-cleaving dioxygenase, Dke1, and cysteine dioxygenase (CDO), and is composed of three histidine residues. The effect of this three-His motif in Dke1 on the geometric and electronic structure of the Fe^{II} center is explored via a combination of absorption, CD, MCD, and VTVH MCD spectroscopies and DFT calculations. This geometric and electronic structure of the three-His triad is compared to that of the classical (2-His-1-carboxylate) facial triad in the α-ketoglutarate (αKG)-dependent dioxygenases clavaminate synthase 2 (CS2) and hydroxyphenylpyruvate dioxygenase (HPPD). Comparison of the ligand fields at the Fe^{II} shows little difference between the three-His and 2-His-1-carboxylate facial triad sites. Acetylacetone, the substrate for Dke1, will also bind to HPPD and is identified as a strong donor, similar to αKG. The major difference between the three-His and 2-His-1-carboxylate facial triad sites is in MLCT transitions observed for both types of triads and reflects their difference in charge. These studies provide insight into the effects of perturbation of the facial triad ligation of the non-heme ferrous enzymes on their geometric and electronic structure and their possible contributions to reactivity.

Mononuclear non-heme iron enzymes (MNHFe's)[1] make up an important class of enzymes that are involved in a wide range of medical, pharmaceutical, and environmental applications. They catalyze a diverse range of chemical reactions, most commonly hydroxylation, but also oxidative ring closure, desaturation, carbon−carbon bond and aromatic ring cleavage, hydrogen atom abstraction, and halogenation (*1*, *3*). The oxygen activating enzymes, including the extradiol dioxygenases, pterin-dependent dioxygenases, Rieske dioxygenases, and α-keto acid-dependent dioxygenases, use Fe^{II} to activate O_2 for attack on the substrate (*1*). They usually share a common structural motif for Fe^{II} coordination: a protein-derived facial triad composed of two histidine residues and one carboxylate moiety (hereafter termed the facial triad) (*4*, *5*). Additionally, along with the substrate, most of these enzymes require a cofactor to deliver the reducing equivalents necessary for reactivity.

Recently, a few exceptions to this facial triad motif have been observed. In the halogenases, the carboxylate is absent and a halogen ion takes its place in the coordination sphere. Diketone-cleaving dioxygenase, Dke1 (*6*), and cysteine dioxygenase, CDO (*7*−*9*), contain a three-histidine triad, while carotenoid oxygenase contains a four-histidine motif. These His-only active site enzymes act directly on their substrates, without the need for a cofactor. Recent work on the NO complex of Cys-bound CDO (*10*) found an $S = {}^1/_2$ site, while the facial triad enzyme ES−NO complexes generally have high-spin, $S = {}^3/_2$ ground states (*11*−*13*). Thus, there can be a ligand field (LF) difference between three-His and facial triad sites, and of course, there are differences between carboxylate and histidine as a ligand. The diketone-cleaving dioxygenase Dke1 from *Acinetobacter johnsonii* cleaves acetylacetone (acac) with incorporation of molecular oxygen to yield methyl glyoxal and acetate (Scheme 1) (*6*). Dke1 will turn over a variety of diketone substrates, and their reaction rates correlate with the energy of the HOMO. The substrate binds directly to the Fe^{II} site in Dke1 which accelerates the rate of reaction with O_2 by $\sim 10^6$-fold. These results indicate the importance of the presence of the Fe^{II}−β-diketone complex in O_2 reactivity (*14*, *15*).

This study elucidates the geometric and electronic structure of the three-His triad in Dke1 and the effects of the acac ligand in binding to the Fe^{II} site. Additionally, the differences between the canonical facial triad motif and the three-His triad are evaluated with comparisons to two well-studied facial triad enzymes, clavaminate synthase (CS2) (*16*) and hydroxyphenylpyruvate dioxygenase (HPPD) (*17*, *18*). In particular, HPPD was chosen for comparison as previous study has shown that it binds β-diketones (*19*).

A combination of spectroscopic techniques and density functional theory (DFT) calculations is used to quantitatively evaluate differences between the three-His triad and the facial triad. Near IR (NIR) circular dichroism (CD), magnetic circular dichroism

†This research was supported by National Institutes of Health Grant GM40392 (E.I.S.) and FWF Grant P18828 (G.D.S.).

*To whom correspondence should be addressed. E.I.S.: e-mail, Edward.solomon@stanford.edu; phone, (650) 723-4694; fax, (650) 725-0259. G.D.S.: e-mail, grit.straganz@tugraz.at; telephone, +43-316-873-8414; fax, +43-316-873-8434.

[1]Abbreviations: MNHFe, mononuclear non-heme iron enzyme; Dke1, diketone-cleaving dioxygenase; CDO, cysteine dioxygenase; LF, ligand field; acac, acetylacetone; CS2, clavaminate synthase 2; HPPD, hydroxyphenylpyruvate dioxygenase; DFT, density functional theory; NIR, near IR; CD, circular dichroism; (VTVH) MCD, (variable-temperature, variable-field) magnetic circular dichroism; MLCT, metal-to-ligand charge transfer; TD-DFT, time-dependent density functional theory; ZFS, zero field splitting.

Published on Web 07/15/2010

Scheme 1: Breakdown of Acetylacetone via Dke1

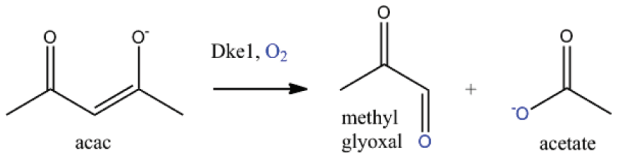

(MCD), and variable-temperature, variable field (VTVH) MCD probe the coordination environment and LF at the Fe^{II} site as explained in the first section of the results. UV−vis absorption, CD, and MCD probe the metal-to-ligand charge transfer (MLCT) transition (of Fe^{II} to acac) and provide insight into the Fe^{II}−acac bond. These studies provide an understanding of the geometric and electronic structure of the three-His triad in Dke1 and the binding of acac to this Fe^{II} site. They also give insight into the utility of the commonly observed facial triad motif in reactivity.

MATERIALS AND METHODS

Sample Preparation. Dke1 and HPPD were purified according to previously published procedures (*6*, *20*, *21*). Apo-dke1 and apo-HPPD were exchanged into deuterated buffer (100 mM Tris-HCl and 100 mM HEPES, respectively) at pD 7.0 using an Ultrafree-4 filter with a 10 kDa cutoff membrane (Millipore) to a concentration of 2−4 mM. All reagents were used as received without further purification. Buffer, acetylacetone, ferrous ammonium sulfate, glycerol-d_3, and sucrose were made anaerobic by purging with Ar on a Schlenk line. Dke1 and HPPD were made anaerobic by alternating cycles of vacuum and purging with Ar at 273 K. All samples were prepared in an inert-atmosphere, N_2-purged "wet box" to maintain an O_2-free environment. Ferrous ammonium sulfate was dissolved in buffer and added to Dke1 or HPPD in microliter quantities to a concentration that was 90% of the enzyme (monomer) concentration to avoid free iron in the sample. Acetylacetone was added in microliter quantities to a concentration that was in 10−25-fold excess over the protein concentration. Glycerol-d_3 (~60%, v/v) or sucrose (175%, w/v) was added to the sample as a glassing agent for MCD measurements, giving a final sample concentration of 1−2 mM. Sucrose was partially deuterated by dissolving in D_2O (1:10, w/v) and incubated overnight, allowing proton−deuteron exchange, and then lyophilized to remove excess water. CD measurements were taken without and with the glassing agent to determine if the glassing agent affects the iron site. For Dke1, a small change in the NIR CD signal was observed with glycerol but not with sucrose. However, MCD measurements on Dke1 with both glycerol and sucrose were identical, indicating that this conformational change does not reflect a change at the iron site. Furthermore, increasing the concentration of acetylacetone in the sample prevented this change in CD without affecting the MCD data. Data presented for Dke1 are with glycerol as the glassing agent because the resulting data have a better signal-to-noise ratio than those of the partially deuterated sucrose. HPPD was not affected by glycerol, and all HPPD MCD samples were made with glycerol-d_3.

Spectroscopic Studies. NIR (600−2000 nm) CD and MCD spectra were recorded on either a Jasco J-200D or Jasco J-730 spectropolarimeter with a liquid N_2-cooled InSb detector (Teledyne Judson Technologies) and an Oxford Instruments SM-4000-7T superconducting magnet. UV−vis (300−900 nm) CD and MCD spectra were recorded on a Jasco J-810D spectropolarimeter equipped with an extended S20 photomultiplier tube and an SM-4000-7T superconducting magnet. UV−vis absorption spectra were recorded on an Agilent 8453 diode array spectrometer. CD and absorption spectra were recorded at 278 K in an anaerobic cuvette and were corrected for buffer and protein baseline effects by subtraction. Natural CD features and baseline effects were excluded from the MCD spectra by taking the average of the magnitudes of the positive and negative field data. For VTVH MCD, a calibrated Cernox resistor (Lakeshore Cryogenics, calibrated at 1.5−300 K), inserted into the sample cell, was used for accurate temperature measurement. The VTVH MCD data obtained were normalized to the intensity maximum, and ground state parameters were obtained using previously published procedures (*22*, *23*).

Computational Methods. The Dke1 active site was modeled using the crystal structure [Protein Data Bank (PDB) entry 3bal] as a starting point. The δ-coordination of one of the histidine residues observed in the crystal structure was preserved. The HPPD active site was modeled using the HPPD−NTBC crystal structure as a starting point (PDB entry 1t47). Histidine residues were truncated to methyl imidazole, and aspartate was truncated to propionate for the models. Constraints imposed by the protein backbone were simulated in both cases by fixing the relative positions of the β-carbons of the backbone. The coordination at the active site was completed with either coordinated water or a monoanionic, bidentate-coordinated acetylacetone ligand.

Density functional theory (DFT) calculations were performed using Gaussian 03 (*24*, *25*) with the spin-unrestricted functional BP86 (*26*) with 10% Hartree−Fock exchange and under tight convergence criteria. The triple-ξ basis set, 6-311G*, was used to describe the Fe and the conjugated O−C−C−C−O moiety of acetylacetone; the double-ξ basis set, 6-31G*, was used to describe all other atoms. The structures were optimized and found to be stable with no imaginary frequencies of $>30\ cm^{-1}$ (which are associated with the constraints placed on the β-carbons). Effects of the protein environment were included by applying the polarized continuum model (PCM) (*27*) with a dielectric constant ($\varepsilon = 4.0$) for calculation of solvated energies for the complexes. These solvated single-point calculations were conducted with the 6-311+G(2d,p) basis set. The energies given include thermal and zero-point corrections. Orbital compositions were determined with QMForge (*28*), and molecular orbitals were visualized with Molden version 4.1 (*29*). Time-dependent DFT (TD-DFT) calculations were performed to compare to the Fe^{II}−acac CT spectra, and SWizard (*30*, *31*) was used to parse the results.

RESULTS

NIR CD and MCD spectroscopy probe the energy splitting of the five d orbitals by the ligand environment (*1*). In a symmetric six-coordinate (6C) site, the d orbitals split into a ground t_{2g} set and excited e_g set separated by $\sim 10000\ cm^{-1}$ for non-heme ligands. The e_g set is further split in energy by the low-symmetry protein environment. 6C Fe^{II} sites exhibit two transitions in the $10000\ cm^{-1}$ region split by $\sim 2000\ cm^{-1}$. For a five-coordinate (5C) site, the splitting is larger, leading to transitions in the ~ 10000 and $5000\ cm^{-1}$ region. For four-coordinate (4C) sites, the ligand field (LF) is weak, leading to transitions in the 5000−$7000\ cm^{-1}$ region. For the high-spin d^6 center in O_h symmetry, the extra electron in the t_{2g} orbitals gives a $^5T_{2g}$ ground state. This is also energy split because of the low symmetry of the protein environment leading to a non-Kramers doublet ground state defined by its zero field splitting (ZFS) δ and $g_{||}$ values. These can be obtained from VTVH MCD data and related to the splitting of

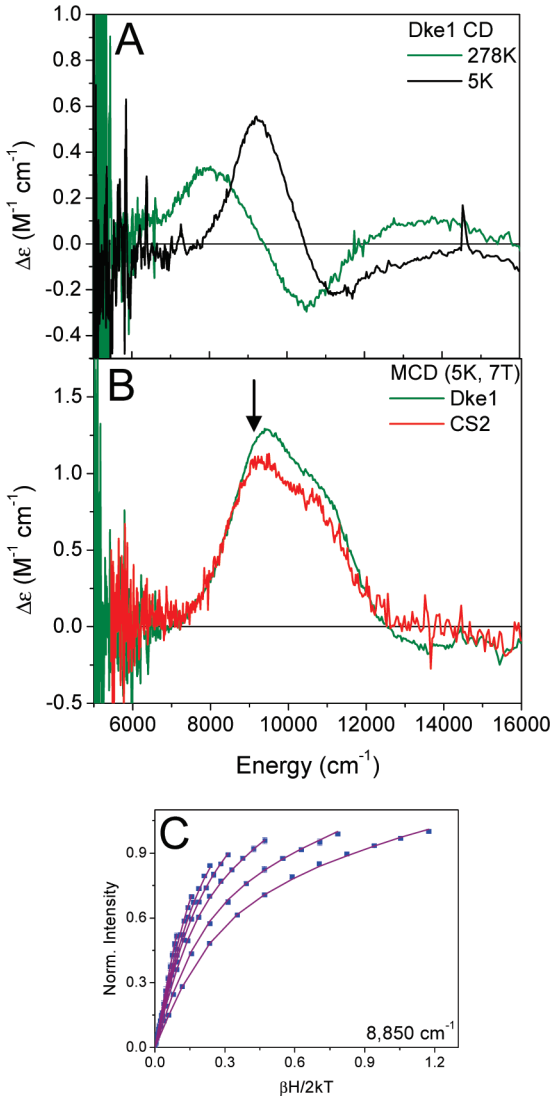

FIGURE 1: CD, MCD, and VTVH MCD of resting Fe^{II}-bound Dke1: (A) 278 and 5 K CD spectra, (B) 7 T, 5 K MCD spectra of resting Fe^{II}-bound Dke1 (green) and CS2 (red), and (C) VTVH MCD isotherms taken at 8850 cm^{-1}.

the t_{2g} set of d orbitals (Δ, the axial splitting, and V, the rhombic splitting) as described in ref *23*.

Resting Dke1. The 278 K CD spectrum of apoDke1 is featureless. Upon addition of 0.9 equiv of Fe^{II}, two transitions are observed in the CD spectrum, a positive feature at 8000 cm^{-1} and a negative feature at 10500 cm^{-1}. When samples are cooled to 5 K, these features sharpen and shift up in energy to ~9000 and ~11000 cm^{-1} (Figure 1A). The 7 T, 5 K MCD spectrum shows two transitions (Figure 1B, green), centered at 10100 cm^{-1}, split by 1600 cm^{-1}. These can be resolved into transitions at 9100 and 10900 cm^{-1}, consistent with the low-temperature CD and indicative of a distorted 6C iron center. To characterize the ground state of this 6C site, VTVH MCD data were taken at 8850 cm^{-1} (arrow in Figure 1B and plotted in Figure 1C). The data fit to a negative zero field splitting with a δ of 4.6 ± 0.2 cm^{-1} and a $g_{||}$ of 9.1 ± 0.3 which leads to a Δ of −300 ± 100 cm^{-1} and a $|V|$ of 140 ± 40 cm^{-1}.

A comparison of the MCD spectrum of Dke1 to the MCD spectrum of a "typical" facial triad enzyme, clavaminate synthase (CS2) (*16*), shows no significant spectral difference (Figure 1B, red). The ground state of Fe-loaded Dke1 also does not show significant differences from the ground state of CS2 (δ = 4.5 ± 0.15 cm^{-1}, and $g_{||}$ = 9.2 ± 0.1, giving Δ = −400 ± 100 cm^{-1} and $|V|$ = 190 ± 50 cm^{-1}). These similarities of the resting sites are shown quantitatively in the experimentally derived ligand field energy level diagram given in Scheme 2 (left).

acac-Bound Dke1 and HPPD. (*i*) *NIR Studies of acac-Bound Dke1 and HPPD*. Addition of acetylacetone (acac) to Fe^{II}-bound Dke1 leads to a large change in the NIR CD and MCD spectra, most notably, the presence of a LF transition at low energy. The 278 K NIR CD spectrum of acac-bound Dke1 (Figure 2A) shows transitions at < 6000 and 13000 cm^{-1}, with the 13000 cm^{-1} peak exhibiting a tail to lower energy. In the corresponding MCD spectrum (Figure 2B), three transitions are clearly observed: a low-energy transition at < 6000 cm^{-1} and two transitions at 9300 and 11000 cm^{-1} with additional asymmetry at the high-energy side of the 11000 cm^{-1} peak. From this asymmetry and the presence of a strong peak in the CD spectrum on the higher-energy side of this band, it can be inferred that there are three transitions in this 8000−13000 cm^{-1} energy region. As a single Fe^{II} center can have no more than two transitions in the NIR region, the presence of a total of four transitions indicates that more than one species is present. From the low-energy band and three transitions in the higher-energy region, a 5C and a 6C site are present. The 6C component has two transitions in the 10000 cm^{-1} region, and the 5C component has one transition in the ~10000 cm^{-1} region and one transition at < 6000 cm^{-1}. VTVH MCD data taken at 9025 cm^{-1} (arrow in Figure 2B and plotted in Figure 2C) fit to a negative zero field split system with the following ground state splitting parameters: δ = 2.6 ± 0.1 cm^{-1}, and $g_{||}$ = 9.0 ± 0.1, giving Δ = −850 ± 100 cm^{-1} and $|V|$ = 400 ± 58 cm^{-1} (consistent with a 6C site but with a weak axial water ligand).[2] VTVH MCD data taken at 11100 cm^{-1} fit to the same parameters as obtained for the 9025 cm^{-1} transition (Figure S1 of the Supporting Information), indicating that these are the two LF transitions of the 6C component. The difference in the ground state splitting parameters between resting Dke1 and the 6C component of the Dke1−acac complex indicates that this 6C component results from having acac bound and does not reflect the unligated resting enzyme. Furthermore, assignment of the two middle transitions to a 6C site allows assignment of the transitions at < 6000 and ~13000 cm^{-1} to a 5C square pyramidal site. Ground state splitting parameters could not be obtained from VTVH MCD data for the 5C species because of noise in the low-energy region and overlap with the 6C site for the higher-energy transition.

To evaluate the effect of the three-His triad relative to the facial triad, spectroscopic studies on an acac-bound facial triad Fe^{II} enzyme were also performed. Hydroxyphenylpyruvate dioxygenase (HPPD) was chosen for these studies because the diketone herbicide NTBC, an inhibitor of HPPD, has been shown to bind to its Fe^{II} center (*32*, *33*). The 278 K CD spectrum of acac-bound HPPD (Figure 2D) is different from the spectrum of the resting enzyme (Figure S2 of the Supporting Information) (*18*) showing one predominant, asymmetric transition at ~12000 cm^{-1}. The 5 K, 7 T MCD spectrum shows three transitions (Figure 2E): two positive features, at < 5000 and ~9000 cm^{-1}, and a negative feature at ~12000 cm^{-1}. Note that the positive intensity to higher energy is an intense CT transition in the MCD spectrum further

[2]The observed splitting of the ^5E excited state indicates that the site is 6C. The ground state, however, shows a fairly large axial splitting indicative of an elongation of the axial $Fe^{II}-H_2O$ bond (*1*).

Scheme 2: Experimentally Derived Ligand Field Diagrams for Resting Dke1 and CS2 (left) and acac-Bound Dke1 and HPPD (right)[a]

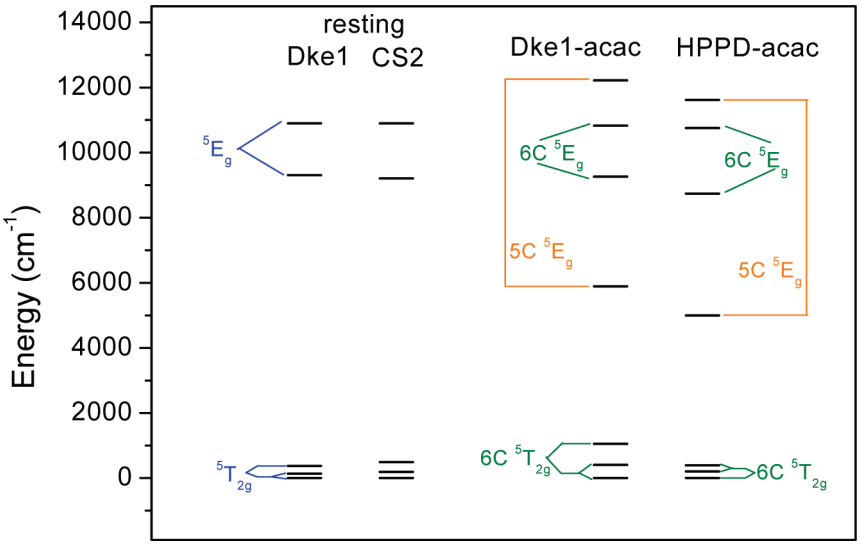

[a]For resting Dke1 and CS2, the ^5E_g and $^5T_{2g}$ states and splittings are colored blue. For acac-bound Dke1 and HPPD, the ^5E_g and $^5T_{2g}$ states and splittings for the 6C site are colored green. The ^5E_g splitting for the 5C sites is colored orange. [The $^5T_{2g}$ splittings for 5C acac-bound Dke1 and HPPD are not shown because the $^5T_{2g}$ splittings for the Dke1−acac complex (5C) could not be obtained as described in the text.]

described in the next section. Again, the presence of more than two transitions indicates that a mixture of two different Fe^{II} sites is present with the low-energy positive−high-energy negative bands characteristic of a 5C square pyramidal site.[3] The middle transition is assigned to a 6C, distorted octahedral component where the second transition is likely masked by the large negative feature from the 5C site. VTVH MCD data for the 6C site taken at ~8600 cm^{-1} (arrow in Figure 2E and plotted in Figure 2F) are best fit to a positive zero field split system ($D = 14 \pm 0.5$ cm^{-1}, and $|E| = 2.7 \pm 0.1$ cm^{-1}, giving $\Delta = 300 \pm 100$ cm^{-1} and $|V| = 192 \pm 64$ cm^{-1}). These splittings are different from those obtained for the 6C component of resting HPPD (*18*), indicating that the 6C component of acac-bound HPPD is an acac-bound species and not an unreacted resting state. VTVH MCD saturation magnetization curves could not be obtained for the low-energy band; however, data taken on the negative band at ~12300 cm^{-1} (Figure S1 of the Supporting Information) are best fit to a negative zero field split system characteristic of a 5C site ($\delta = 2.3 \pm 0.2$ cm^{-1}, and $g_{||} = 8.9 \pm 0.1$, giving $\Delta = -1000 \pm 100$ cm^{-1} and $|V| = 540 \pm 60$ cm^{-1}). The experimental ligand field energy splittings obtained from the analysis described above for both Dke1−acac and HPPD−acac complexes are shown in Scheme 2 (right side).

(*ii*) *UV−Vis Spectra of acac-Bound Dke1 and HPPD.* The acac−Fe^{II} complex of Dke1 has a MLCT transition in the UV−vis region. The UV−vis absorption, CD, and MCD spectra (Figure 3) of Dke1−acac and HPPD−acac complexes were obtained to probe this MLCT transition for both classes of NH Fe enzymes with the same substrate. A single, broad transition assigned to this MLCT is observed at ~24000 cm^{-1} in all three spectra of the Dke1−acac complex. In the HPPD−acac complex, this transition is shifted to lower energy by ~1000 cm^{-1} and is less intense than the transition in the Dke1−acac complex. A second transition is observed at a higher energy (~28000 cm^{-1}) for the acac complexes of both enzymes which is assigned as an intraligand transition (vide infra).

Nature of the acac−Fe^{II} Bond. The HOMO of the acac ligand is an out-of-plane π orbital with maximum density at the central carbon. The LUMO is an out-of-plane π^* orbital with significant carbonyl character (Figure S3 of the Supporting Information). These orbitals are positioned for good overlap with the Fe^{II} center similar to the bonding defined for the α-keto acid moiety in ref *33*.

DFT studies of the three His−acac (Dke1 model) and facial triad−acac (HPPD model) complexes were performed to aid in the assignment of the transitions and the description of bonding. Molecular orbital energy level diagrams (Figure 4, spin-unrestricted, α orbitals on the left, β orbitals on the right) of the three His− and facial triad−acac complexes show that the acac HOMO and LUMO orbitals are close in energy to the Fe d orbitals. The contours in Figure 5 show that these are oriented to interact with the Fe^{II} d orbitals. The amount of acceptor π^* LUMO character in the donor d_{xz} orbital reflects the amount of Fe^{II} backbonding into the acac ligand, and this backbonding determines the strength of the MCLT transition. From the calculations, the amount of π^* character in the donor d_{xz} orbital is similar for both the three His− and facial triad−acac complexes (~5−6%); however, the experimentally observed MLCT transition of acac-bound Dke1 is more intense than that of acac-bound HPPD (Figure 3). This intensity difference suggests that there is more Fe^{II} backbonding with the three-His triad and that the calculations slightly underestimate the overlap in the three His−acac complex versus the facial triad−acac complex.

Time-dependent DFT (TD-DFT) calculations were performed to correlate to the MLCT transition in the UV−vis absorption spectrum. As both the 5C and 6C sites will contribute to the MLCT transition, spectra were calculated for both coordination numbers in both the three His− and facial triad−acac models. (All four predicted spectra and the Gaussian resolution of the

[3]Although most of the ferrous proteins that have been studied show only positively signed d−d transitions in MCD [due to ground state spin orbit coupling (see ref *22*)], in a few cases a negative higher-energy transition is observed. The negative transition arises from spin orbit coupling between the components of the split E excited state due to a distortion of the LF which results in d_π/d_σ mixing and occurs in distorted 5C, square pyramidal sites (*2*).

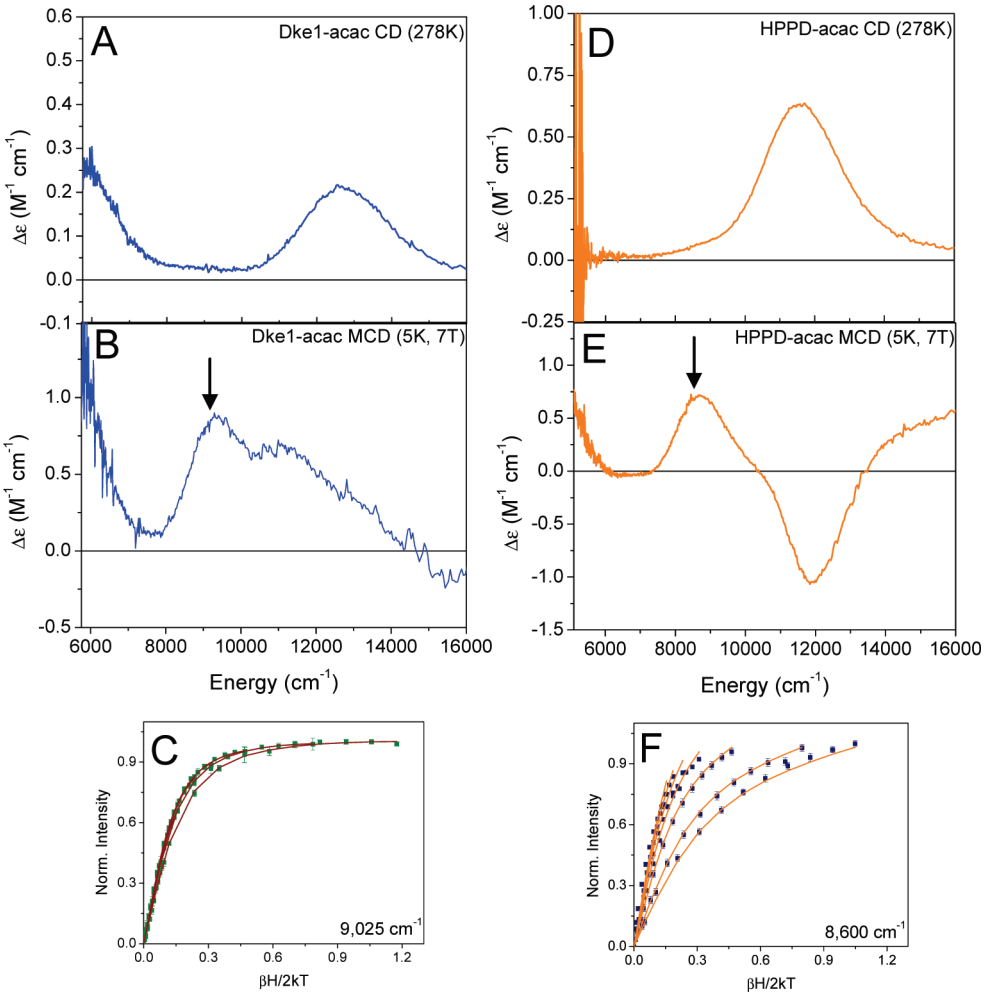

FIGURE 2: CD, MCD, and VTVH MCD of acac-bound complexes. (A and D) The 278 K CD spectra of Fe^{II}−Dke1−acac (A) and Fe^{II}−HPPD−acac (D) complexes. (B and E) the 7 T, 5 K MCD spectra of Fe^{II}−Dke1−acac (B) and Fe^{II}−HPPD−acac (E) complexes. (C and F) VTVH MCD isotherms taken at 9025 and 8600 cm^{-1} for Dke1 (C) and HPPD (F), respectively.

major bands are in Figure S4 of the Supporting Information.) The TD-DFT calculations predict the observed dπ → acac π^* MLCT transition and an intraligand (π to π^*, acac HOMO → LUMO) transition for the acac-bound models. Additionally, the TD-DFT calculations predict the energy shift observed experimentally with the MLCT transition for the three His (Dke1)−acac complex that is higher in energy than this transition in the facial triad (HPPD)−acac complex by ~3000 cm^{-1}.

DISCUSSION

The Three-His Ligand Field. As imidazole is a stronger field ligand than carboxylate, a change in the Fe^{II} coordinating ligand set from a carboxylate oxygen to histidine nitrogen could suggest that the ligand field would change as well. Additionally, the low spin, $S = {}^1/_2$ state that is observed in the cysteine-bound CDO−NO (*10*) complex potentially also suggests that the ligand field of the three His triad may be higher than in the facial triad. However, this in fact is not observed for Dke1 as the experimentally derived ligand field splitting of the d orbitals in Scheme 2 is very similar to that of the "typical" 6C facial triad/H_2O coordination observed experimentally in CS2. This reflects the fact that only one of six ligand positions is perturbed. Furthermore, DFT calculations with a facial triad−NO complex with cysteine bound in the orientation proposed previously for CDO (coordination through the thiolate and the amine) indicate that the facial triad−cysteine−NO complex would also be a low-spin form. This supports the previous assertion that it is the cysteine ligand that drives the CDO−NO complex to a low-spin state (*10*). Thus, it is unlikely that the ligand field of the three-His triad would significantly affect the spin state energetics along the reaction coordinate relative to the facial triad.[4]

acac−Fe^{II} Bond. Many of the resting facial triad sites are 6C. On comparison of a three-His triad and a facial triad, a three-His triad is a poorer donor. Thus, it is not surprising that the resting site of Dke1 is also found to be 6C (Figure 1). When acac binds, the affinity for water is decreased due to the strong π donation from the acac ligand. Indeed, from the calculated structures, the energy required to remove a H_2O ligand (water affinity) for acac-bound Dke1 is lower than for water bound to resting Dke1 by ~2.8 kcal/mol (see Figure S5A,B of the Supporting Information). Therefore, a 6C to 5C conversion occurs in Dke1 upon acac substrate binding and opens up a coordination position for reaction with O_2.

The parallel comparison can be made for the facial triad and αKG. acac is a similar anionic π donor to αKG, and thus, it might be expected that the water affinity in an αKG-bound facial triad would be low. Indeed, calculations predict loss of H_2O and

[4]The effect of δ versus ε coordination by the His ligand was also examined. No significant geometric, electronic, or energetic effects resulted from this change.

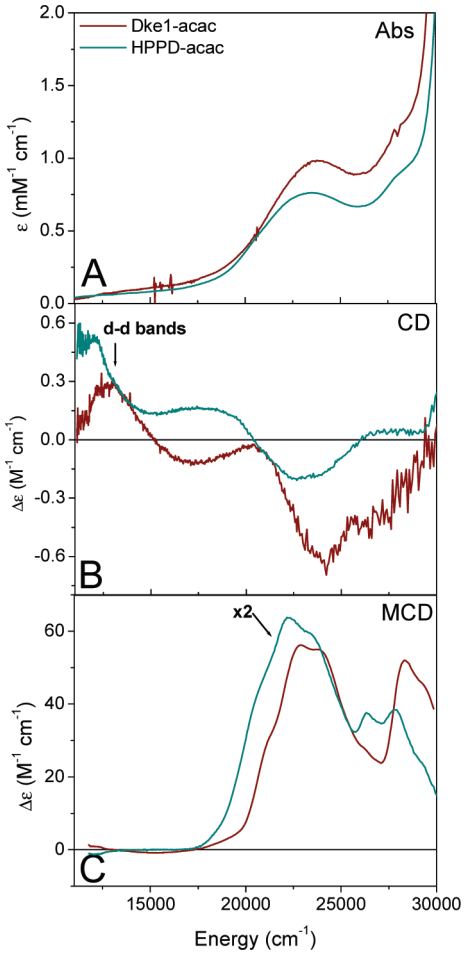

FIGURE 3: UV−vis absorption, CD, and MCD spectra of acac-bound complexes: (A) room-temperature absorption spectra, (B) room-temperature CD spectra, and (C) 7 T, 5 K MCD spectra of Fe^{II}−Dke1−acac (maroon) and Fe^{II}−HPPD−acac (teal, x2) complexes.

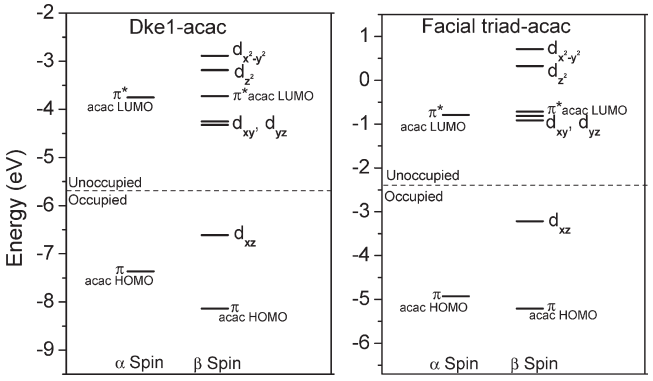

FIGURE 4: Molecular orbital energy level diagrams for 5C three His−acac and facial triad−acac complexes.

the formation of a 5C site with αKG bound [$\Delta G = -13$ kcal/mol (see Figure S5C of the Supporting Information)]. However, from previous spectroscopic and crystallographic studies on αKG-dependent enzymes, a 6C site is commonly found for the αKG-bound site. However, in these enzymes, the coordinated water hydrogen bonds to the noncoordinated oxygen of the carboxylate. The calculated water affinity for a hydrogen-bonded structure increases 8−9 kcal/mol [ΔG (Figure S5D of the Supporting Information), in agreement with previously calculated values (*34*). This is important for enzymes such as CS2 in which uncoupled

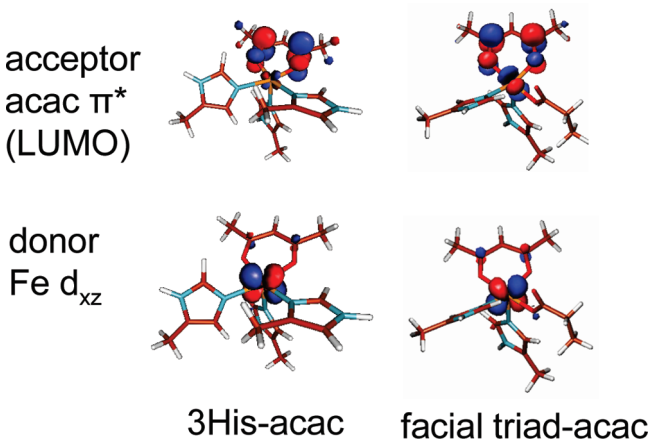

FIGURE 5: Molecular orbital contours for the donor and acceptor orbitals for MCLT.

reactivity would occur if a 5C site is formed with αKG bound before substrate is present. Addition of substrate provides the sterics for elimination of the coordinated water and allows the reaction with O_2 in these substrate- plus cofactor-dependent enzymes. It should be noted that HPPD is a special case because in HPP the α-keto acid is covalently tethered to the substrate and therefore binds as both the cofactor and substrate. Interestingly, the resting site of HPPD is already partially 5C, and it was suggested that the carboxylate of the facial triad in HPPD is poorly oriented for hydrogen bonding with the coordinated water due to interactions from a conserved phenylalanine residue (*18*). Thus, in HPPD, the site is prearranged to disrupt hydrogen bonding between the facial triad carboxylate and coordinated water allowing HPP and, in our study, acac to drive the site to go 5C.

Charge. The dominant difference in the spectrum of the three-His triad relative to that of the facial triad is in the energy of the MLCT transition, which reflects the charge difference of these two sites. The higher positive charge at the three-His center decreases the energy of the d manifold, resulting in the shift to higher energy of its Fe^{II}-to-acac MLCT transition (Figure 3). Consistent with a higher positive charge on the Fe^{II} of the three-His triad, studies on the effect of pH on Dke1 showed a depressed pK_a for bound water (~8.2) (*35*) relative to the facial triad which does not show deprotonation in the accessible pH range.

Mechanistic implications can be posited from this difference in charge. First, the differences in charge between the three-His and facial triads could affect the nature of substrate binding, in particular for α-keto acid where both mono- and dianions are accessible. The facial triad found in the α-keto acid enzymes binds this cofactor as the monoanion. Studies on model complexes by Que and co-workers (*36*) suggest that a dianionic, enolized α-keto acid would react with O_2 to give cleavage products different from the keto form. The proposed mechanism for this reaction would not generate an Fe^{IV}=O intermediate. However, this intermediate is observed and is required in the α-keto acid-dependent non-heme Fe enzyme reactivity. The lower positive charge at the active site with a facial triad likely helps stabilize the keto form of this cofactor, leading to the required Fe^{IV}=O intermediate and subsequent H atom abstraction reactivity.

In summary, the facial triad, as a ligand set for Fe^{II}, is conserved throughout most members of the oxygen activating class of mononuclear non-heme iron enzymes. The three-His triad in Dke1 presents an opportunity not only to study the role of the Fe^{II}−three His active site in the cleavage of *β*-diketones but also

to make comparisons to the facial triad ligand set in a functional environment. It has a ligand field similar to that of the facial triad. While most of the facial triad enzymes require both cofactor and substrate to bind for 6C to 5C conversion, acac binding to the three-His site alone eliminates a coordinated water generating a 5C site and opens a position for O_2 reactivity. Finally, the difference in charge between the three-His and facial triad ligand sets, which leads to the major spectral difference observed, could play a key mechanistic role in promoting the proper form of αKG binding and thus O_2 reactivity in the facial triad. Future studies will explore the effects of this difference in charge on reactivity.

SUPPORTING INFORMATION AVAILABLE

Full citation for ref *24*, VTVH MCD isotherms for the Dke1−acac complex at 11100 cm^{-1} and the HPPD−acac complex at 12300 cm^{-1}, CD and MCD of the resting Fe^{II}−HPPD complex, HOMO and LUMO of free acac, TD-DFT predicted spectra for acac-bound complexes, and structures used to calculate water affinity. This material is available free of charge via the Internet at http://pubs.acs.org.

REFERENCES

1. Solomon, E. I., Brunold, T. C., Davis, M. I., Kemsley, J. N., Lee, S. K., Lehnert, N., Neese, F., Skulan, A. J., Yang, Y. S., and Zhou, J. (2000) Geometric and electronic structure/function correlations in non-heme iron enzymes. *Chem. Rev. 100*, 235–349.
2. Davis, M. I., Wasinger, E. C., Decker, A., Pau, M. Y. M., Vaillancourt, F. H., Bolin, J. T., Eltis, L. D., Hedman, B., Hodgson, K. O., and Solomon, E. I. (2003) Spectroscopic and electronic structure studies of 2,3-dihydroxybiphenyl 1,2-dioxygenase: O_2 reactivity of the non-heme ferrous site in extradiol dioxygenases. *J. Am. Chem. Soc. 125*, 11214–11227.
3. Neidig, M. L., and Solomon, E. I. (2005) Structure-function correlations in oxygen activating non-heme iron enzymes. *Chem. Commun.,* 5843–5863.
4. Koehntop, K. D., Emerson, J. P., and Que, L. (2005) The 2-His-1-carboxylate facial triad: A versatile platform for dioxygen activation by mononuclear non-heme iron(II) enzymes. *J. Biol. Inorg. Chem. 10*, 87–93.
5. Hegg, E. L., and Que, L. (1997) The 2-His-1-carboxylate facial triad: An emerging structural motif in mononuclear non-heme iron(II) enzymes. *Eur. J. Biochem. 250*, 625–629.
6. Straganz, G. D., Glieder, A., Brecker, L., Ribbons, D. W., and Steiner, W. (2003) Acetylacetone-cleaving enzyme Dke1: A novel C-C-bond-cleaving enzyme from *Acinetobacter johnsonii*. *Biochem. J. 369*, 573–581.
7. McCoy, J. G., Bailey, L. J., Bitto, E., Bingman, C. A., Aceti, D. J., Fox, B. G., and Phillips, G. N. (2006) Structure and mechanism of mouse cysteine dioxygenase. *Proc. Natl. Acad. Sci. U.S.A. 103*, 3084–3089.
8. Yamaguchi, K., Hosokawa, Y., Kohashi, N., Kori, Y., Sakakibara, S., and Ueda, I. (1978) Rat-Liver Cysteine Dioxygenase (Cysteine Oxidase): Further Purification, Characterization, and Analysis of Activation and Inactivation. *J. Biochem. 83*, 479–491.
9. Gardner, J. D., Pierce, B. S., Fox, B. G., and Brunold, T. C. (2010) Spectroscopic and Computational Characterization of Substrate-Bound Mouse Cysteine Dioxygenase: Nature of the Ferrous and Ferric Cysteine Adducts and Mechanistic Implications. *Biochemistry 49*, 6033–6041.
10. Pierce, B. S., Gardner, J. D., Bailey, L. J., Brunold, T. C., and Fox, B. G. (2007) Characterization of the nitrosyl adduct of substrate-bound mouse cysteine dioxygenase by electron paramagnetic resonance: Electronic structure of the active site and mechanistic implications. *Biochemistry 46*, 8569–8578.
11. Brown, C. A., Pavlosky, M. A., Westre, T. E., Zhang, Y., Hedman, B., Hodgson, K. O., and Solomon, E. I. (1995) Spectroscopic and Theoretical Description of the Electronic-Structure of S = 3/2 Iron-Nitrosyl Complexes and Their Relation to O_2 Activation by Nonheme Tron Enzyme Active-Sites. *J. Am. Chem. Soc. 117*, 715–732.
12. Brown, C. D., Neidig, M. L., Neibergall, M. B., Lipscomb, J. D., and Solomon, E. I. (2007) VTVH-MCD and DFT studies of thiolate bonding to $\{FeNO\}^7/\{FeO_2\}^8$ complexes of isopenicillin N synthase: Substrate determination of oxidase versus oxygenase activity in nonheme Fe enzymes. *J. Am. Chem. Soc. 129*, 7427–7438.
13. Ye, S., Price, J. C., Barr, E. W., Green, M. T., Bollinger, J. M., Krebs, C., and Neese, F. (2010) Cryoreduction of the NO-Adduct of Taurine: α-Ketoglutarate Dioxygenase (TauD) Yields an Elusive $\{FeNO\}^8$ Species. *J. Am. Chem. Soc. 132*, 4739–4751.
14. Straganz, G. D., Hofer, H., Steiner, W., and Nidetzky, B. (2004) Electronic substituent effects on the cleavage specificity of a non-heme Fe^{2+}-dependent β-diketone dioxygenase and their mechanistic implications. *J. Am. Chem. Soc. 126*, 12202–12203.
15. Straganz, G. D., and Nidetzky, B. (2005) Reaction coordinate analysis for β-diketone cleavage by the non-heme Fe^{2+}-dependent dioxygenase Dke1. *J. Am. Chem. Soc. 127*, 12306–12314.
16. Pavel, E. G., Zhou, J., Busby, R. W., Gunsior, M., Townsend, C. A., and Solomon, E. I. (1998) Circular dichroism and magnetic circular dichroism spectroscopic studies of the non-heme ferrous active site in clavaminate synthase and its interaction with α-ketoglutarate cosubstrate. *J. Am. Chem. Soc. 120*, 743–753.
17. Neidig, M. L., Decker, A., Choroba, O. W., Huang, F., Kavana, M., Moran, G. R., Spencer, J. B., and Solomon, E. I. (2006) Spectroscopic and electronic structure studies of aromatic electrophilic attack and hydrogen-atom abstraction by non-heme iron enzymes. *Proc. Natl. Acad. Sci. U.S.A. 103*, 12966–12973.
18. Neidig, M. L., Kavana, M., Moran, G. R., and Solomon, E. I. (2004) CD and MCD studies of the non-heme ferrous active site in (4-hydroxyphenyl)pyruvate dioxygenase: Correlation between oxygen activation in the extradiol and α-KG-dependent dioxygenases. *J. Am. Chem. Soc. 126*, 4486–4487.
19. Brownlee, J. M., Johnson-Winters, K., Harrison, D. H. T., and Moran, G. R. (2004) Structure of the ferrous form of (4-hydroxyphenyl)pyruvate dioxygenase from *Streptomyces avermitilis* in complex with the therapeutic herbicide, NTBC. *Biochemistry 43*, 6370–6377.
20. Straganz, G., Brecker, L., Weber, H. J., Steiner, W., and Ribbons, D. W. (2002) A novel β-diketone-cleaving enzyme from *Acinetobacter johnsonii*: Acetylacetone 2,3-oxygenase. *Biochem. Biophys. Res. Commun. 297*, 232–236.
21. Johnson-Winters, K., Purpero, V. M., Kavana, M., Nelson, T., and Moran, G. R. (2003) (4-hydroxyphenyl)pyruvate dioxygenase from *Streptomyces avermitilis*: The basis for ordered substrate addition. *Biochemistry 42*, 2072–2080.
22. Pavel, E. G., Kitajima, N., and Solomon, E. I. (1998) Magnetic circular dichroism spectroscopic studies of mononuclear non-heme ferrous model complexes. Correlation of excited- and ground-state electronic structure with geometry. *J. Am. Chem. Soc. 120*, 3949–3962.
23. Solomon, E. I., Pavel, E. G., Loeb, K. E., and Campochiaro, C. (1995) Magnetic Circular-Dichroism Spectroscopy as a Probe of the Geometric and Electronic-Structure of Nonheme Ferrous Enzymes. *Coord. Chem. Rev. 144*, 369–460.
24. Frisch, M. J., et al. (2007) Gaussian 03, revision E.01, Gaussian, Inc., Waterbury, CT.
25. Perdew, J. P. (1986) Density-Functional Approximation for the Correlation-Energy of the Inhomogeneous Electron-Gas. *Phys. Rev. B 33*, 8822–8824.
26. Becke, A. D. (1988) Density-Functional Exchange-Energy Approximation with Correct Asymptotic-Behavior. *Phys. Rev. A 38*, 3098–3100.
27. Cramer, C. J., and Truhlar, D. G. (1999) Implicit solvation models: Equilibria, structure, spectra, and dynamics. *Chem. Rev. 99*, 2161–2200.
28. Tenderholt, A. L. (2007) QMForge, version 2.1.
29. Schaftenaar, G., and Noordik, J. H. (2000) Molden: A pre- and post-processing program for molecular and electronic structures. *J. Comput.-Aided Mol. Des. 14*, 123–134.
30. Gorelsky, S. I. (2010) SWizard.
31. Gorelsky, S. I., and Lever, A. B. P. (2001) Electronic structure and spectral, of ruthenium diimine complexes by density functional theory and INDO/S. Comparison of the two methods. *J. Organomet. Chem. 635*, 187–196.
32. Kavana, M., Purpero, V. M., and Moran, G. R. (2003) Studies of the interaction of streptomyces avermitilis (4-hydroxyphenyl)pyruvate dioxygenase with the specific inhibitor NTBC. *J. Inorg. Biochem. 96*, 166–166.
33. Neidig, M. L., Decker, A., Kavana, M., Moran, G. R., and Solomon, E. I. (2005) Spectroscopic and computational studies of NTBC bound to the non-heme iron enzyme (4-hydroxyphenyl)pyruvate dioxygenase: Active site contributions to drug inhibition. *Biochem. Biophys. Res. Commun. 338*, 206–214.
34. Neidig, M. L., Brown, C. D., Light, K. M., Fujimori, D. G., Nolan, E. M., Price, J. C., Barr, E. W., Bollinger, J. M., Krebs, C., Walsh, C. T., and Solomon, E. I. (2007) CD and MCD of CytC3 and taurine

dioxygenase: Role of the facial triad in α-KG-dependent oxygenases. *J. Am. Chem. Soc. 129*, 14224–14231.

35. Straganz, G. D., Diebold, A. R., Egger, S., Nidetzky, B., and Solomon, E. I. (2010) Kinetic and CD/MCD Spectroscopic Studies of the Atypical, Three-His-Ligated, Non-Heme Fe^{2+} Center in Diketone Dioxygenase: The Role of Hydrophilic Outer Shell Residues in Catalysis. *Biochemistry 49*, 996–1004.
36. Paine, T. K., England, J., and Que, L. (2007) Iron-catalyzed C2-C3 bond cleavage of phenylpyruvate with O_2: Insight into aliphatic C-C bond-cleaving dioxygenases. *Chem.—Eur. J. 13*, 6073–6081.